Article

J. Mex. Chem. Soc. **2021**, *65*(2)
Regular Issue

ISSN-e 2594-0317

Effect of Bathocuproine Concentration on the Photovoltaic Performance of NiO_x-Based Perovskite Solar Cells

Hamed Moeini Alishah[1*], Fatma Pinar Gokdemir Choi[1], Ugur Deneb Menda[2], Cihangir Kahveci[1], Macide Canturk Rodop[1], Manuel J. Mendes[2], Serap Gunes[1]

[1]Yildiz Technical University, Faculty of Arts and Science, Department of Physics, Davutpasa Campus, 34210, Esenler/Istanbul/Turkey.
[2]i3N/CENIMAT, Department of Materials Science, Faculty of Science and Technology, Universidade NOVA de Lisboa and CEMOP/UNINOVA, Campus de Caparica, 2829-516 Caparica, Portugal.

***Corresponding author:** Hamed Moeini Alishah, email: hamed.moeini.alishah@gmail.com, phone: +90 2123834231; Fax: +90 2123834234

Received October 15th, 2020; Accepted December 9th , 2020.

DOI: http://dx.doi.org/10.29356/jmcs.v65i2.1461

Abstract. Bathocuproine (BCP) (2,9-dimethyl-4,7-diphenyl-1,10-phenanthroline) is a well-known material that is employed as a hole-blocking layer between electron transport layer (ETL) and metal electrode in perovskite solar cells. It has been demonstrated that the use of BCP as a buffer layer between the ETL and the metal electrode in perovskite solar cells is highly beneficial. In literature, BCP is coated using vacuum processing techniques. Vacuum processing techniques require more energy and cost-effective processing conditions. In this work, we used BCP layers processed through wet processing techniques using sol-gel method with different concentrations. We achieved a *short circuit current density (J_{sc}) of 16.1 mA/cm^2* and *an open circuit voltage (V_{oc}) of 875 mV* were acquired and a *fill factor (FF) of 0.37* was calculated for perovskite solar cells without a BCP layer leading to a power conversion efficiency *(PCE) of 5.32 %* whereas *J_{sc} of 19 mA/cm^2*, *V_{oc} of 990 mV* were achieved and a *FF of 0.5* was calculated for perovskite solar cells employing BCP layers with concentration of 0.5 mg/ml and spin cast at 4000 rpm, leading to a PCE of *9.4 %*. It has been observed that the use of a BCP layer with an optimized concentration led to an improved device performance with an increase of *77 % in PCE* in ambient air under high humidity conditions for planar structure perovskite solar cells in the configuration of ITO/NiO_x/$MAPbI_3$/PCBM/BCP/Ag.
Keywords: Bathocuproine; hole-blocking layer; electron transport layer; planar structure.

Resumen. Batocuproina (BCP) (2,9-dimetil-4,7-difenil-1,10-fenantrolina) es un material que se emplea como capa de bloqueo de huecos entre la capa transportadora de electrones (ETL) y el electrodo metálico en celdas solares basados en perovskitas. Se ha demostrado que el uso de BCP como capa amortiguadora entre el ETL y el electrodo metálico en las celdas solares de perovskita es beneficioso. Comúnmente el BCP se recubre mediante técnicas de procesamiento al vacío, las cuales requieren altos costos energéticos. En este trabajo utilizamos capas de BCP procesadas mediante técnicas de procesamiento húmedo utilizando el método sol-gel. Logramos una densidad de corriente de cortocircuito (Jsc) de 16.1 mA / cm^2 y un voltaje de circuito abierto (Voc) de 875 mV y se calculó un factor de llenado (FF) de 0.37 para las celdas solares de perovskita sin una capa de BCP lo que conduce a una eficiencia de conversión de energía (PCE) de 5.32%. Para celdas solares de perovskita que emplean capas de BCP con concentración de 0.5 mg/ml y centrifugado a 4000 rpm el valor de Jsc fue de 19 mA / cm^2, se lograron Voc de 990 mV y se calculó un FF de 0.5, lo que lleva a un PCE del 9,4%. Se observó que el uso de una capa de BCP con concentración optimizada puede conducir a un rendimiento

J. Mex. Chem. Soc. **2021**, *65*(2)
Regular Issue

ISSN-e 2594-0317

mejorado del dispositivo con un aumento del 77% en PCE en el aire ambiente, en condiciones de alta humedad, para celdas solares de perovskita de estructura plana en la configuración de ITO / NiOx / MAPbI3 / PCBM / BCP / Ag.
Palabras clave: Batocuproina; capa de bloqueo de huecos; capa transportadora de electrones; estructura plana.

Introduction

Perovskite solar cells possess great capabilities such as low cost, high power efficiency possessing perovskite materials with long diffusion length, high mobility, tunable band gap, low exciton binding energy, high absorption coefficient [1-7]. Due to the cost and energy efficient production techniques for fabrication of perovskite solar cells, they are super foreseen as competitors of silicon solar cells [8,9] and are regarded as coming alternatives of silicon-based solar cells [8,10,11]. Perovskite solar cells can be fabricated in two different configurations of n-i-p or p-i-n. n-i-p configuration consists of an electron transport layer (ETL), perovskite semiconductor material, and a hole transport layer (HTL) whereas in the p-i-n, which is also regarded as inverted type perovskite solar cells, a hole transport layer, perovskite layer and an electron transport layer are employed. P-i-n structures serve several advantages such as lower processing temperatures and the use of well-known fullerenes as electron transport layers [12-14]. In the p-i-n structure, nickel oxide (NiO_x) received very much attention among researchers since NiO_x provides good stability and possesses high hole mobility [15-16]. Generally, buffer layers such as bathocuproine (BCP) [17-20], LiF [21,22], polyethyleneimine (PEIE) [23] are used in p-i-n structure of perovskite solar cells to hinder recombination between ETL and cathode.

Thin BCP films as buffer layers can be processed through vacuum or solution. Although there are various number of studies based on BCP layers processed through vacuum [24-27], the number of studies on solution processed BCP layers is rather limited [28-31]. In this work, we studied the effect of BCP layers on the performance of perovskite solar cells by changing the BCP concentration, which was prepared by sol-gel method and also, we have studied the effect of spin-coating speed of BCP layers on the performance of perovskite solar cells in p-i-n configuration as ITO/NiO_x/$MAPbI_3$/PCBM/BCP/Ag configuration (Fig. 1) in ambient air under high humidity (~ *60%*) conditions. This method, unlike previous ones, does not require a high vacuum system.

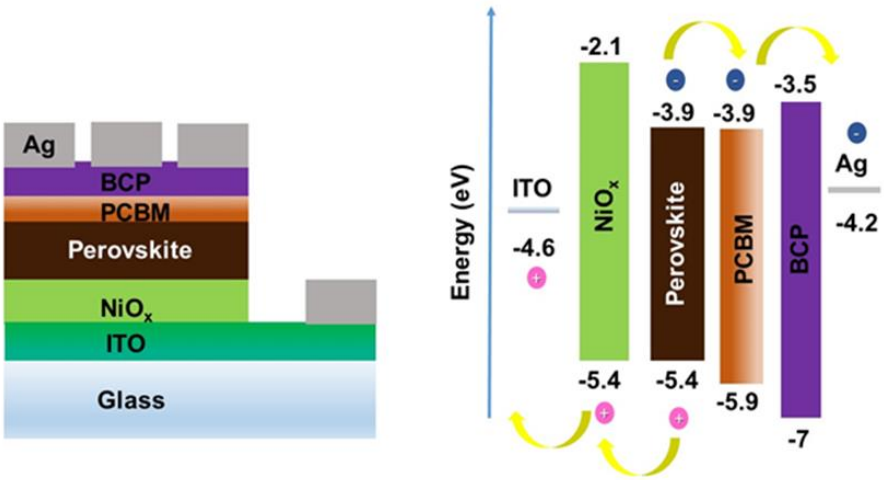

Fig. 1. (a) Schematic description and **(b)** Energy level diagram for the device.

J. Mex. Chem. Soc. **2021**, *65*(2)
Regular Issue

ISSN-e 2594-0317

Experimental

Materials

PbI_2 (lead iodide, Sigma-Aldrich 99.0%), methylammonium iodide (CH_3NH_3I (MAI), Lumtec 99.99%), Nickel (II) acetate tetrahydrate (Sigma, ≥99.0%), BCP (2,9-dimethyl-4,7-diphenyl- 1,10-phenanthroline, 96%, Sigma), PCBM ([6, 6]-phenyl-C61-butyric acid methyl ester, Solenne, 99%), were purchased and used without further purification.

Device fabrication

124.42 mg nickel (II) acetate tetrahydrate was dissolved in *5 ml* isopropanol and *30 µl* ethanolamine (MEA) mixture at room temperature. The mixture was stirred at *70 °C* for at least two hours to get NiO_x solution. This solution is filtered with a *0.22* micrometer PTFE filter prior to spin casting. Perovskite solution was prepared by mixing MAI:PbI_2 with a molar ratio of *1.4:1.4* in γ-butyrolactone (GBL) and stirred at *65 °C* for at least *6* hours and was filtered with a *0.45 µm* PTFE filter. Different concentrations of bathocuproine (BCP) were dissolved in absolute ethanol. PCBM solution was achieved by dissolving *20 mg* PCBM powder in *1 ml* chlorobenzene (CB) and stirring at room temperature for *2* hours.

For fabrication of devices initially, one-third of ITO coated glasses were etched by a mixture of $HCl:HNO_3:H_2O$ (*4.6:0.4:5*) acid solution and were cleaned by ethanol, acetone and isopropanol, respectively. Then they were sonicated separately in acetone (for *20* minutes) and isopropanol (for *45* minutes at *60 °C*) to remove any kind of impurities on the surface. Finally, substrates were dried by N_2 gas.

NiO_x solution was spin coated at *1500 rpm* for *30* seconds at room temperature and coated substrates dried at *80 °C* on a hot plate for *15* minutes and then coating repeated once more. Finally, NiO_x layers were annealed in a muffle furnace at *450 °C* for *30* minutes and used without any UV-ozone treatment. Perovskite film was achieved by spin coating the perovskite solution at *2000 rpm* for *10* seconds and *4000 rpm* for *20* seconds. While the rotation speed approached *4000 rpm*, toluene washing was applied to get crystalline perovskite film. Thereafter, thermal annealing at *100 °C* for *20* minutes was applied. PCBM solution was cast at *1500 rpm* for *30* seconds, then dried at *90 °C* for *90* seconds. BCP solutions with different concentrations (*0.325 mg/ml*, *0.5 mg/ml*, *1 mg/ml*, *2 mg/l* and *4 mg/ml*) were spin coated at two different spinning speeds, *1500 rpm* and *4000 rpm* for *40* seconds, separately. Finally, *110 nm* thick Ag was coated by thermal evaporation method.

Characterization

Keithley 2400-LV source meter with LabVIEW software were used for achieving current density-voltage (*J-V*) curves of devices under illumination of *100 mW/cm²* to simulate the condition of AM 1.5. Open-circuit voltage ($V_{OC}(V)$), short-circuit current density (J_{sc} *(mA/cm²)*), fill factor (*FF*) were determined from *J-V* curves. Fill factor is given by following formula:

$$FF = \frac{V_{mpp} \times J_{mpp}}{V_{oc} \times J_{sc}} \quad (1)$$

And the power conversion efficiency (*PCE*) of device was determined by the ratio of power-out to power-in as following formula:

$$PCE(\%) = \left(\frac{P_{out}}{P_{in}}\right) \times 100 = \left(\frac{FF \times V_{oc} \times J_{sc}}{P_{in}}\right) \times 100 \quad (2)$$

I-V curve of solar cell can be calculated in presence of shunt and series resistance as follow

J. Mex. Chem. Soc. **2021**, *65*(2)
Regular Issue

ISSN-e 2594-0317

$$I = I_L - I_0 \exp\left[\frac{q(V+IR_s)}{nK_BT}\right] - \frac{V+IR_s}{R_{sh}} \quad (3)$$

where, I_L is light generated current, I_0 is saturated current, T is temperature, n is ideality factor, R_s is series resistance, R_{sh} is shunt resistance, k_B is Boltzmann's constant, and q is electronic charge.

Incident photon to current efficiency (*IPCE*) was performed with New Port measurement system, which contains optical system consisting of a xenon lamp, a filter wheel, mechanical chopper, and a monochromator. The absorption spectra of perovskite film were achieved by using a Perkin Elmer Lambda 950 UV-VIS spectrometer. Crystalline structure of perovskite layers observed by a PANalytical Xpert PRO MRD X-ray diffractometer. FTIR spectra of the perovskite layer recorded with a Thermo Nicolet 6700 spectrometer. Photoluminescence spectroscopy of perovskite layer was achieved by using PerkinElmer LS 55 Luminescence spectrometer.

Results and discussion

Fig. 2 shows the XRD pattern of the perovskite layer. The peaks refer to characteristic peaks of crystalline perovskite ($MAPbI_3$) structure. *2θ = 13.98°*, *28.32°* and *31.74°*, *40.5°* and *42.5°* correspond to the (*110*), (*220*), (*310*), (*224*) and (*330*) planes, which indicate the formation of the tetragonal perovskite structure [32].

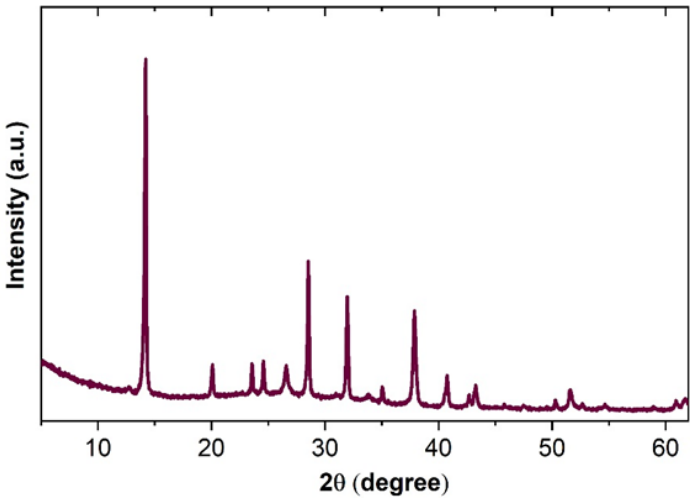

Fig. 2. XRD of perovskite ($MAPbI_3$) film.

Fig. 3 shows UV-Vis absorption and photoluminescence spectra (PL) of perovskite film. The obtained optical band gap of $MAPbI_3$ is *1.61 eV* which is consistent with the reported values [33-35].

J. Mex. Chem. Soc. **2021**, *65*(2)
Regular Issue

ISSN-e 2594-0317

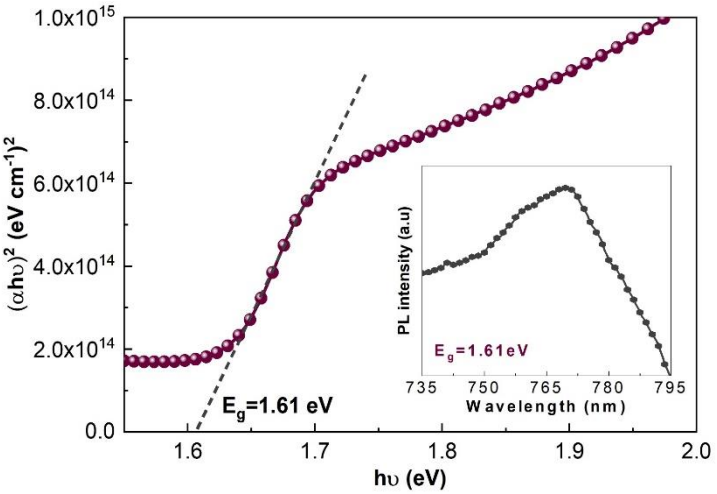

Fig. 3. UV-Vis absorption spectra and photoluminescence (PL) of perovskite ($MAPbI_3$) film.

Fig. 4 shows the FTIR spectra of perovskite film coated on ITO substrate. The FTIR spectrum tells about what functional groups present in the molecule. The IR band at *1465* cm^{-1} is mainly attributed to C–H band bending in alkane group. The IR band at *3180* cm^{-1} and *3138* cm^{-1} belongs to N–H stretching bond [36-37].

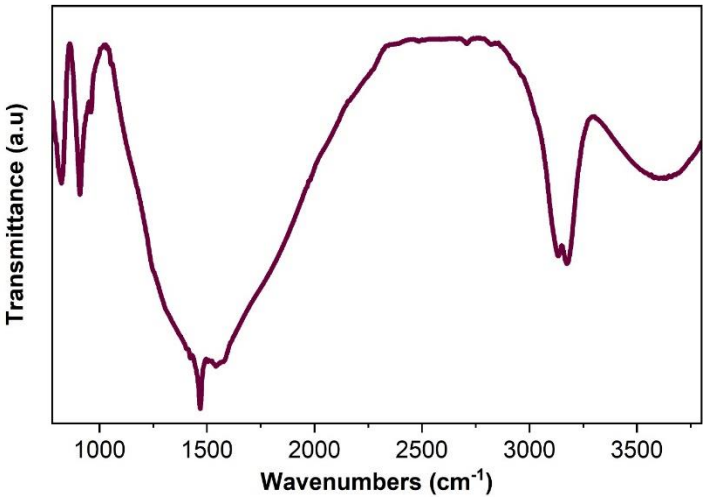

Fig. 4. FTIR spectra of ITO/perovskite ($MAPbI_3$) film.

Fig. 5 (**a**)-(**b**) shows the current density-voltage (*J-V*) curves of devices consisting of BCP layers, prepared with different concentrations and spinning speeds of *1500 rpm* and *4000 rpm*, respectively. The J_{sc} of the devices increased as the concentration of BCP increased to *0.5 mg/ml*. As the concentration of BCP is further increased to *2 mg/ml* we have observed a reduction in the PV performance of the devices. BCP, Lithium fluoride (LiF) and Ca are widely used in literature as an interfacial layer [38]. They help to prevent the energy mismatch between cathode and electron transport layer and also to prevent the diffusion of cathode to the conducting under-layers, which may lead to recombination [38].

J. Mex. Chem. Soc. **2021**, *65*(2)
Regular Issue

ISSN-e 2594-0317

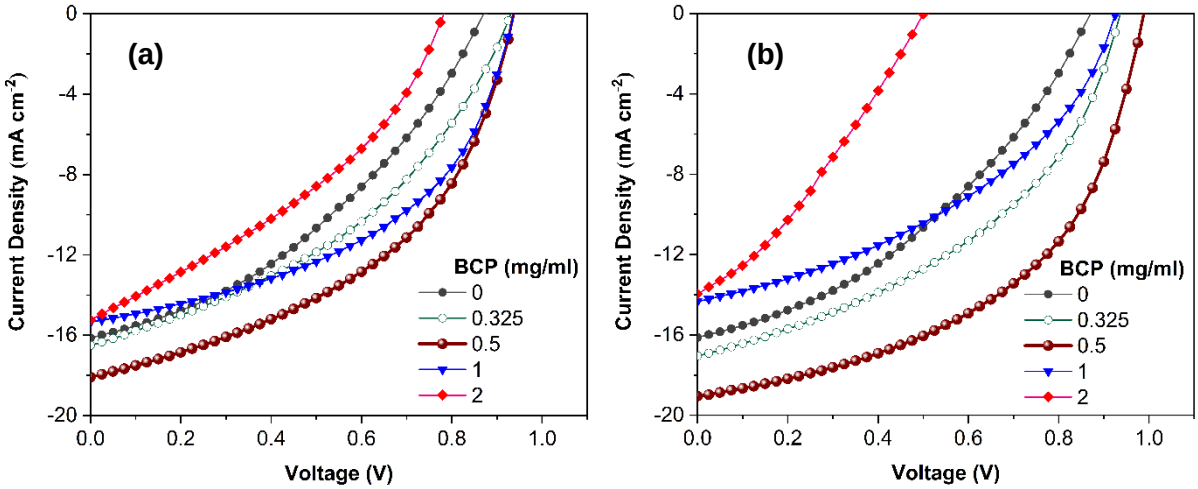

Fig. 5. Current density-voltage curves of the solar cell devices as a function of BCP precursor concentration cast at **(a)** *1500 rpm* and **(b)** *4000 rpm* spinning speeds.

Fig. 6 (**a**) shows the *PCE* of the devices with different concentrations of BCP solution cast at *1500 rpm* and *4000 rpm*. Spin coating is a procedure used to deposit uniform thin films onto flat substrates. Usually a small amount of coating material is applied on the center of the substrate. The substrate is rotated at different speeds to spread the coating material by centrifugal force. Variations in the speed of the spin coating directly affect the thickness of the thin films. Thinner films can be achieved as the spinning speeds are increased. Keeping the BCP concentration constant, we have achieved a higher efficiency when BCP layer is cast at higher spinning speeds of *4000 rpm*. Higher spinning speeds lead to thinner films. Therefore, we expect a thinner BCP film for *4000 rpm* as compared to *1500 rpm*. Please note that the BCP layer is an interfacial layer between ETL and the metal contact therefore if the BCP layer is too thin or too thick, charge accumulation will emerge due to different mechanisms and lead to device performance degradation [39]. We have chosen intermediate low and high spinning speeds as *1500 rpm* and *4000 rpm* and demonstrated that the *4000 rpm* is the proper spinning speed for BCP layers. The devices containing BCP layers cast from *0.5 mg/ml* concentration at *4000 rpm* exhibit the highest efficiency of all. We have observed that the concentration of BCP solution significantly affected the performance of PSCs. As concentration increased, the power conversion efficiency (*PCE*) of the PSCs increased at first and then decreased [19].

Fig. 6 (**b**) shows the series resistance (R_s) of devices. As can be seen the R_s is minimum for devices containing BCP layers with *0.5 mg/ml* concentration in both spinning speeds. For devices with no BCP layer, between PCBM and Ag Schottky contact can be formed [40]. Schottky contact causes charge accumulation and large series resistance, which lead to low performance of devices. When a thin layer of BCP is placed between PCBM and Ag, R_s is decreased due to formation of an ohmic contact [18]. Thus, the concentration of BCP plays a significant role in the performance of the perovskite devices since viscosity of a solution depends on concentration of dissolved substance [41] and viscosity plays a critical role in thickness of coated film [42]. Due to the insulating feature of BCP, high concentration of BCP could lead to hindering of charge transfer at the interface. It has been observed in literature that too thin or thick BCP layers lead to charge accumulation through different mechanisms, which cause to low device performance [43].

J. Mex. Chem. Soc. **2021**, *65*(2)
Regular Issue

ISSN-e 2594-0317

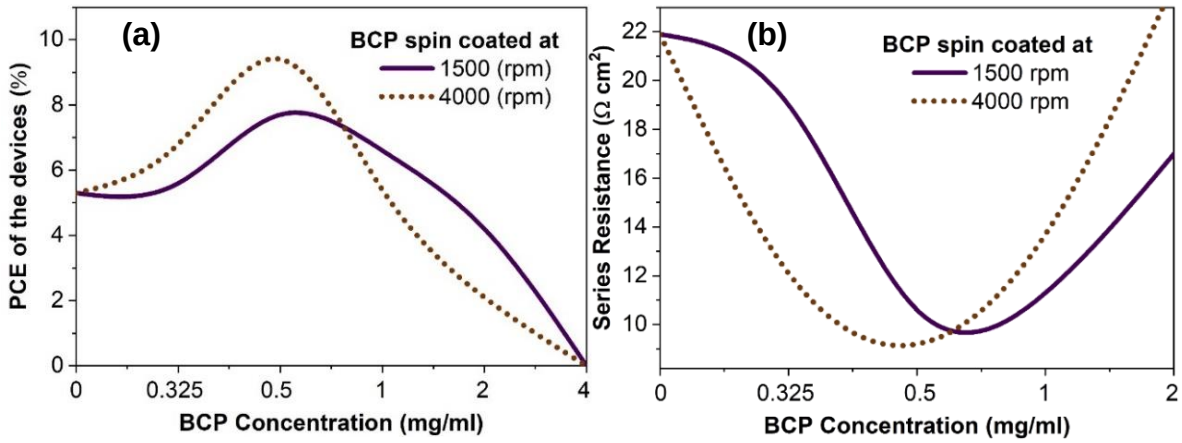

Fig. 6. (a) Power conversion efficiency and **(b)** series resistance of the solar cell devices as a function BCP layer coating parameters.

We have fabricated electron-only (e-only) devices in the configuration of ITO/TiO_2/Perovskite/PCBM/BCP/Ag and as a comparison we have also fabricated a control e-only device without BCP. Fig. 7 (**a**) and (**b**) show the *J-V* dark *J-V* characteristics of perovskite solar cells and e-only devices with and without BCP. As can be seen from Fig. 7 (**a**), the leakage current density is lower for perovskite solar cells with BCP layer respectively. The leakage current originates from the improper interfacial contact near the contact layer [29] and may reflect the interface condition at some extent. The lower dark current suggests a better interfacial modification by BCP. As can be seen from Fig. 7 (**b**), the current increases linearly with voltage up to a kink point. A rise in the current is observed as the voltage is increased above the kink point, which demonstrates the filling of the trap states by injected carriers [44] We have determined the trap densities by using the trap-filled limit voltage (V_{TFL}) using the equation:

$$V_{TFL} = \frac{en_t L^2}{2\varepsilon\varepsilon_0} \quad (4)$$

where, n_t is the trap-state density, L is the thickness of the perovskite film, e, ε and ε_0 are the elementary charge and permittivity of the perovskite and vacuum, respectively. Dielectric constant of the perovskite was taken as *32* from the literature [45]. The thickness of perovskite layer was *240 nm*. Trap density was calculated as $5.71x10^{15}\ cm^{-3}$ for the e-only control device without BCP, whereas trap density was calculated as $4.65x10^{15}\ cm^{-3}$ for the e-only device with BCP. As can be seen the trap density is reduced when BCP is introduced in the device configuration, which is an indication of an improved device quality upon BCP addition.

J. Mex. Chem. Soc. **2021**, *65*(2)
Regular Issue

ISSN-e 2594-0317

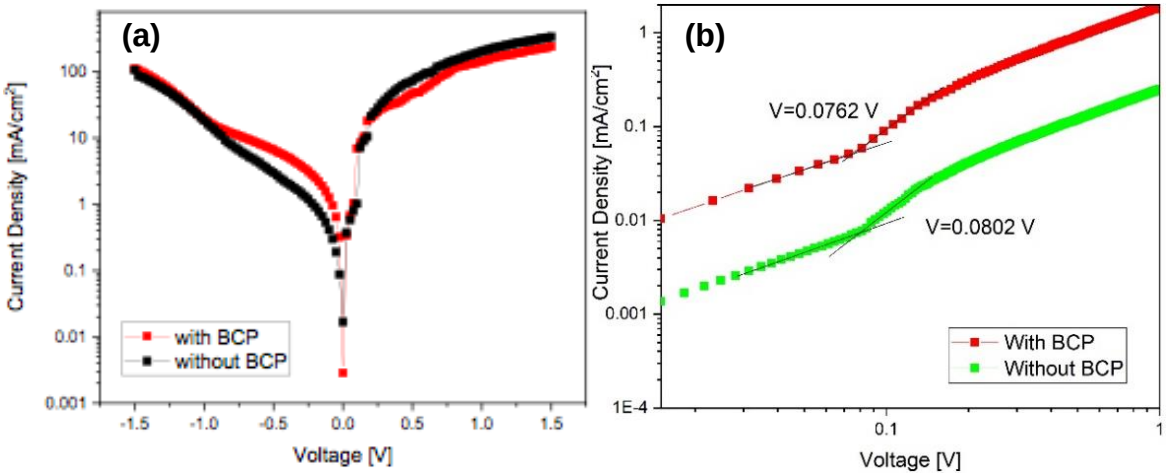

Fig. 7. Dark current density-voltage characteristics of **(a)** perovskite solar cells **(b)** e-only devices (ITO/TiO_2/$MAPbI_3$/PCBM/BCP/Ag) with and without BCP (*0.5 mg/ml, 4000 rpm*) layers.

Table 1 presents the photovoltaic parameters of the herein fabricated devices. It can be seen that employing the BCP decreases the series resistance of devices. Devices without using BCP exhibited a J_{SC} of *16.1 mA/cm*^{2} and a V_{OC} of *0.875 V* with a *0.37* of fill factor, which led to a *PCE* of *5.3 %*. The J_{SC}, V_{OC}, and *FF* increased to *19 mA/cm*^{2}, *0.99 V*, and *0.5*, respectively for devices employing BCP layers prepared from *0.5 mg/ml* concentration, which led to a *PCE* of *9.4 %*. For higher concentrations, the performance of devices showed a significant reduction in the J_{SC}, V_{OC}, and *FF* thereby leading to a lower *PCE*.

Table 1. Photovoltaic parameters of fabricated devices.

BCP (mg/ml)	Casting (rpm)	V_{OC} (mV)	J_{SC} (mAcm^{-2})	FF	PCE (%)	R_S (Ωcm^2)	R_{Sh} (Ωcm^2)
0		875	16.1	0.37	5.32	2.19×10^1	1.9×10^2
0.325	1500	930	16.5	0.37	5.6	1.9×10^1	1.65×10^2
	4000	930	17	0.43	6.8	1.21×10^1	1.79×10^2
0.5	1500	930	18	0.46	7.7	1.06×10^1	1.82×10^2
	4000	990	19	0.50	9.4	0.92×10^1	2.95×10^2
1	1500	930	15.3	0.47	6.6	1.13×10^1	2.52×10^2
	4000	925	14.3	0.41	5.4	1.37×10^1	2.11×10^2
2	1500	780	15.2	0.36	4.2	1.7×10^1	8.84×10^2
	4000	510	13.9	0.30	2.1	2.4×10^1	6.88×10^2

Fig. 8 shows photovoltaic parameter (V_{OC}, J_{SC}, *FF*, *PCE*) statistics of solar cell devices fabricated employing various BCP concentrations at different coating speeds for *15* devices. *FF* and V_{OC} are related to junction properties of perovskite solar cell [19] and higher V_{OC} and *FF* enhance the power conversion efficiency (*PCE*). J_{SC} depends on transferring of generated charge carriers in perovskite layer to the proper transport layer, and if charge carrier transferring does not happen effectively, they will be recombined or accumulated in the interface [46, 47]. As shown in Fig. 7 the current density (J_{SC}) has been significantly improved along with increasing the BCP concentration to *0.5* (*mg/ml*). This result illustrates the mentioned concentration of BCP could reduce recombination at interface. Furthermore, the devices exhibit a good reproducibility.

J. Mex. Chem. Soc. **2021**, *65*(2)
Regular Issue

ISSN-e 2594-0317

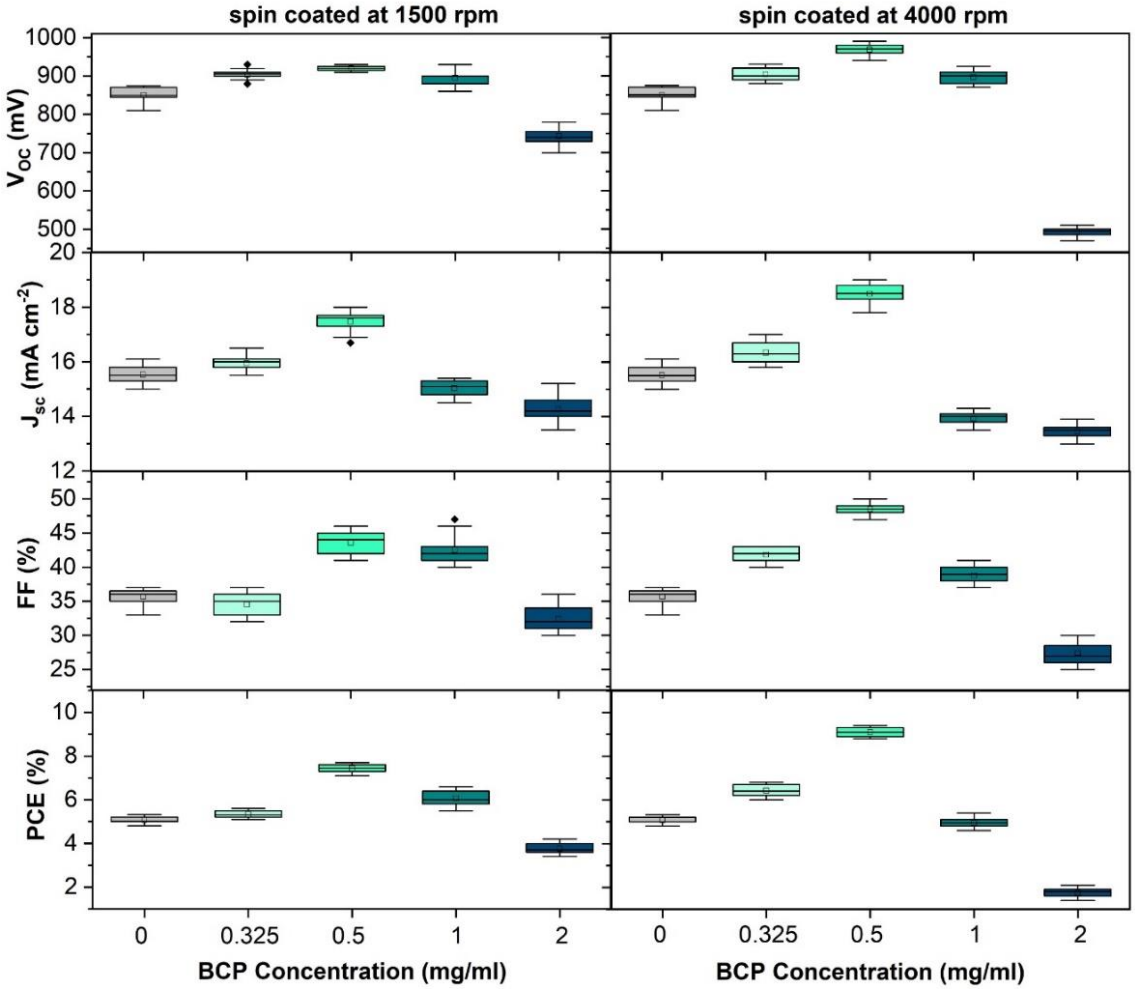

Fig. 8. Distribution of the open circuit voltage, short circuit current density, fill factor and power conversion efficiency values over *15* solar cell devices as a function of different BCP concentrations cast at *1500 rpm* and *4000 rpm.*

Fig. 9 shows the external quantum efficiency (*EQE*) of perovskite solar cells with the optimized BCP layer and without BCP layers. *EQE* is ratio between number of charge carriers generated by photon and collected by device to number of incident photons. Using BCP increased the EQE in both short and long wavelength region. The integrated photocurrent density (J_{SC}) from the *EQE* curve was *16.05 mA/cm*^{2} for PCBM/Ag and *18.7 mA/cm*^{2} for PCBM/BCP (*0.5 mg/ml, 4000 rpm*) /Ag. The J_{SC} achieved by EQE spectra were in good agreement with the J_{SC} obtained from *J-V* measurements. The higher *EQE* in PCBM/BCP(*0.5 mg/ml*) /Ag structure is due to using BCP as a hole-blocking layer which results in reduction in charge carrier recombination at the interface.

J. Mex. Chem. Soc. **2021**, *65*(2)
Regular Issue

ISSN-e 2594-0317

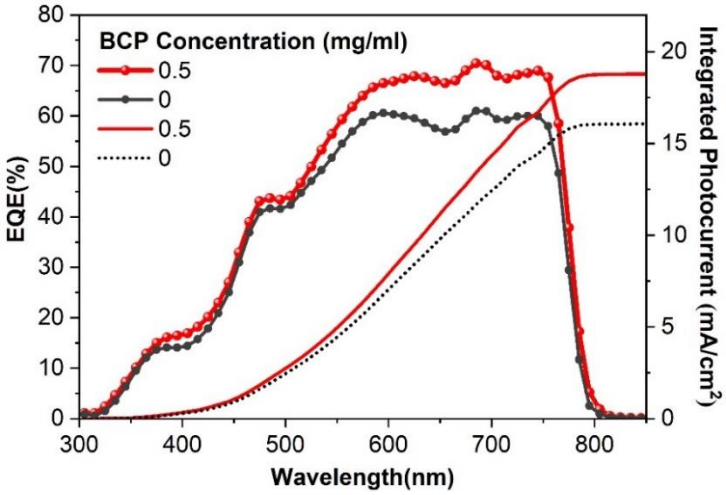

Fig. 9. External quantum efficiencies and corresponded integrated photocurrent densities of the solar cell devices with BCP (*0.5 mg/ml, 4000 rpm*) and without BCP layers.

Conclusion

In summary, inserting a BCP interfacial layer between the electron transporting layer, PCBM, and the metal contact, Ag improved the performance of perovskite solar cells. The best device performance was achieved when *0.5 mg/ml* of BCP concentration was used and spin coated at *4000 rpm*. Further increase in BCP concentration led to thicker films and due to charge accumulation at PCBM and thick BCP interface as observed in the literature [18,19] led to a lower device performance. When the concentration of BCP was optimized, the series resistance of devices decreased which led to improvement in the cell's performance, yielding a best device *PCE* of *9.4%*.

Acknowledgements

This work was financially supported by the FBA-2019-3583 NAP Project of Yildiz Technical University, and the Portuguese Foundation for Science and Technology (FCT/MCTES) under the project SUPERSOLAR (PTDC/NAN-OPT/28430/2017).

References

1. Chen, H.; Yang, S. *Adv. Mater*. **2017**, *29*, 1603994.
2. Shin, G. S.; Choi, W.-G.; Na, S.; Gokdemir, F. P.; Moon, T. *Electron.. Mater. Lett.* **2018,** *14*, 155-160
3. Huanping, Z.; Chen, Q.; Li, G.; Luo, S.; Song, T.-B.; Duan, H.-S.; Hong, Z.; You, J.; Liu, Y.; Yang, Y. *Science* **2014**, *345*, 542-546.
4. Polman, A.; Knight, M.; Garnett, E. C.; Ehrler, B.; Sinke, W. C. *Science* **2016**, *352*, 6283.
5. Lee, M. M.; Teuscher, J.; Miyasaka, T.; Murakami, T. N.; Snaith, H. J. *Science*, **2012**, *338*, 643-647.
6. Brites, M. J.; Barreiros, M. A.; Corregidor, V.; Alves, L. C.; Pinto, J. V.; Mendes, M.J.; Fortunato, E.; Martins, R.; Mascarenhas, J. *ACS Appl. Energy Mater*. **2019**, *2*, 1844-1853.

J. Mex. Chem. Soc. **2021**, *65*(2)
Regular Issue

ISSN-e 2594-0317

7. Laban, W. A.; Etgar, L. *Energy Environ. Sci.* **2013**, *6*, 3249-3253.
8. Seigo, I. *APL Mater.* **2016**, *4*, 091504.
9. Jacoby, M. *Chem. Eng. News* **2016**, *94*, 30-35.
10. Miyasaka, T. *Bull. Chem. Soc. Jpn* **2018**, *91*, 1058-1068.
11. Wiley, A. D.-S.; Zhou, Y.; P. Padture, N.; Mitzi, D. B. *Chem. Rev.* **2018**, *119*, 3193-3295.
12. Alishah, H. M.; Kazici, M.; Ongul, F.; Bozar, S.; Canturk Rodop, M.; Kahveci,, C.; Arvas M. B.; Sahin, Y.; Gencten, M.; Kaleli, M.; Akyurekli, S.; Yilmaz, H. U.; Bayram, A. B.; Gunes, S. *J. Mater. Sci.: Mater. Electr.* **2020**, 1-13.
13. Dericiler, K.; Alishah, H. M.; Bozar, S; Gunes, S; Kaya, F. *Appl. Phys. A* **2020**, *126*, 1-9.
14. Choi, F. P. G.; Alishah, H. M.; Bozar, S.; Doyranli, C.; Koyuncu, S.; San, N.; Kahveci, C.; Rodop, M. C.; Arvas, M. B.; Gencten, M.; Sahin, Y.; Gunes, S. *Sol. Energy* **2020**, *209*, 400-407.
15. Chen, W.; Liu, F.-Z.; Feng, X.-Y.; Djurišić, A. B.; Chan, W. K.; He, Z.-B. *Adv. Energy Mater.* **2017**, *7*,1700722.
16. Sajid, S.; Elseman, A. M.; Huang, H.; Ji, J.; Dou, S.; Jiang, H.; Liu, X.; Wei, D.; Cui, P.; Li, M. *Nano Energy* **2018**, *51*, 408-424.
17. Jeng, J.-Y.; Chiang, Y.-F.; Lee, M.-H.; Peng, S.-R.; Guo, T.-F.; Chen, P.; Ten-Chin, W. *Adv. Mater.* **2013**, *25*, 3727-3732.
18. Shibayama N.; Kanda H.; Kim T. W.; Segawa H.; Ito S. APL Materials, **2019**, 7.3: 031117.
19. Chen, C.; Zhang, S.; Wu, S.; Zhang, W.; Zhu, H.; Xiong, Z.; Zhang, Y.; Chen, W., *RSC Adv.* **2017**, *7*, 35819-35826.
20. Patil, B. R.; Ahmadpour, M.; Sherafatipour, G.; Qamar, T.; Fernández, A. F.; Zojer, K.; Rubahn, H.-G.; Madsen, M. *Sci. Rep.* **2018**, *8*, 1-9.
21. Seo, J.; Park, S.; Kim, Y. C.; Jeon, N. J.; Noh, J. H.; Yoon, S. C.; Seok, S. I. *Energy Environ. Sci.* **2014**, *7*, 2642-2646.
22. Liu, X.; Yu, H.; Yan, L.; Dong, Q.; Wan, Q.; Zhou, Y.; Song, B.; Li, Y. *ACS Appl. Mater. Interfaces* **2015**, 7.11: 6230-6237.
23. Guo, F.; Azimi, H.; Hou, Y.; Przybilla, T.; Hu, M.; Bronnbauer, C.; Langner, S.; Spiecker, E.; Forberich, K.; Brabec, C. J. *Nanoscale* **2015**, *7*, 1642-1649.
24. He, C.; Zhang, F.; Zhao, X.; Lin, C.; Ye, M. *Front. Phys.* **2018**, 6, 99.
25. Wang, Q.; Shao, Y.; Dong, Q.; Xiao, Z.; Yuan, Y.; Huang, J. *Energy Environ. Sci.* **2014**, 2359-2365.
26. Hanmandlu, C.; Chen, C. Y.; Boopathi, K. M.; Lin, H. W.; Lai, C. S.; Chu, C. W. *ACS Appl. Mater. Interfaces* **2017**, *9*, 32635-32642.
27. Babaei, A.; Dreessen, C.; Sessolo, M.; Bolink, H. J. *RSC Adv.* **2020**, *10*, 6640-6646.
28. Wang, Y.; Zhang, J.; Wu, Y.; Yi, Z.; Chi, F.; Wong, H.; Li, W.; Zhang, Y.; Zhang, X.; Liu, L. *Semicond. Sci. Technol.* **2019**, *34*, 075023.
29. Yuan, D. X.; Yuan , X. D.; Xu, Q. Y.; Xu, M. F.; Shi, X. B.; Wang, Z. K.; Liao, L. S. *Phys. Chem. Chem. Phys.* **2015**, *17*, 26653-26658.
30. Di Girolamo, D.; Matteocci, F.; Lamanna, E.; Calabrò, E.; Di Carlo, A.; Dini, D. *AIP Conf. Proc.* **2018**, *1990*, 020011.
31. Wang, T.; Ding, D.; Zheng, H.; Wang, X.; Wang, J.; Liu, H.; Shen, W. *Solar RRL*, **2019**, *3*, 1900045.
32. Guo, X.; McCleese, C.; Kolodziej, C.; Samia, A. CS; Zhao, Y.; Burda, C. *Dalton Trans.* **2016**, *45*, 3806-3813.
33. Leguy, A. M. A. ; Azarhoosh, P.; Alonso, M. I.; Campoy-Quiles, M.; Weber, O. J.; Yao, J.; Bryant, D; Weller, M..T; Nelson, J; Walsh, A; Schilfgaarde, M.V; Barnes, P.R.F. *Nanoscale* **2016**, *8*, 6317-6327.

J. Mex. Chem. Soc. **2021**, *65*(2)
Regular Issue

ISSN-e 2594-0317

34. Quarti, C.; Mosconi, E.; Ball, J. M.; D'Innocenzo, V.; Tao, C.; Pathak, S.; Snaith, H. J.; Petrozza, A.; Angelis, F. D. *Energy Environ. Sci.* **2016**, *9*, 155-163.
35. Kojima, A.; Teshima, K.; Shirai, Y.; Miyasaka, T. *J. Am. Chem. Soc.* **2009**, *131*, 6050-6051.
36. Patel, J. B.; Milot, R. L.; Wright, A. D.; Herz, L. M.; Johnston, M. B. *J. Phys. Chem. Lett.* **2016**, *7*, 96-102.
37. Pérez-Osorio, M. A.; Milot, R. L.; Filip, M. R.; Patel, J. B.; Herz, L. M.; Johnston, M. B.; Giustino, F. *J. Phys. Chem. C* **2015**, *119*, 25703-25718.
38. Hu, H.; Kollek, T.; Hanusch, F.; Polarz, S.; Docampo, P.; Schmiidt-Mende, L. *Molecules* **2016**, *21*, 542.
39. Chen, C.; Zhang, S.; Wu, S.; Zhang, W.; Zhu, H.; Xiong, Z.; Zhang, Y.; Chen, W. *RSC Adv.* **2017**, *7*, 35819-35826.
40. Yan, K.; Wei, Z.; Li, J.; Chen, H.; Yi, Y.; Zheng, X.; Long, X; Wang, Z; Wang, J; Xu, J; Yang, S. *Small* **2015**, *11*, 2269-2274.
41. Yimsiri, P.; Mackley, M. R. *Chem. Eng. Sci.* **2006**, *61*, 3496-3505.
42. Calleja, A.; Ricart, S.; Aklalouch, M.; Mestres, N.; Puig, T.; Obradors, X. *J. Sol-Gel Sci.Technol.* **2014**, *72*, 21-29.
43. Dong, J.; Xu, X.; Shi, J.-J.; Li, D.-M.; Luo, Y.-H.; Meng, Q.-B.; Chen, Q. *Chin. Phys. Lett.* **2015**, *32*, 078401.
44. Wu, X.; Li, H.; Wang, K.; Sun, X.; Wang, L. *RSC Adv.* **2018**, *8*, 11095-11101.
45. Zhu, W.; Kang, L.; Yu, T.; Lv, B.; Wang, Y.; Chen, X.; Wang, X,; Zhou, Y.; Zou, Z., *ACS Appl. Mater. Interfaces* **2017**, *9*, 6104-6113.
46. Yamada, Y.; Nakamura, T.; Endo, M.; Wakamiya, A.; Kanemitsu, Y. *J. Am. Chem. Soc.* **2014**, *136*, 11610-11613.
47. Han, G.S.; Chung, H.S.; Kim, B.J.; Kim, D.H.; Lee, J.W.; Swain, B.S.; Mahmood, K.; Yoo, J. S.; Park, N.-G.; Lee, J.H.; Jung, H.S. *J. Mater. Chem. A*, **2015**, *3*, 9160-9164.